Q. J. R. Meteorol. Soc. (1999), **125**, pp. 2153–2170

On the removal of the effect of horizontal fluxes in two-aircraft measurements of cloud absorption

By ALEXANDER MARSHAK[1]*, WARREN WISCOMBE[2], ANTHONY DAVIS[3], LAZAROS OREOPOULOS[1] and ROBERT CAHALAN[2]

[1]*University of Maryland Baltimore County, USA*
[2]*NASA – Goddard Space Flight Center, USA*
[3]*Los Alamos National Laboratory, USA*

(Received 4 June 1998; revised 2 November 1998)

SUMMARY

Cloud absorption inferred from the difference between the net fluxes measured by stacked aircraft below and above clouds is strongly affected by the uncertainties due to cloud horizontal inhomogeneity. The simplest way to get rid of these uncertainties is to perform grand averages over flight legs; if flight legs are long enough, grand averaging may lead to a reliable estimate of cloud absorption. However, the amount of information on 'true' cloud absorption returned from such an expensive measurement program will be very limited—often one number per flight leg.

This paper contains a discussion on how to enhance the harvest of true absorption data using two related methods: (a) subtraction and (b) conditional sampling. Both methods assume that, simultaneously with broad-band measurements, some narrow non-absorbing-band net flux measurements are also available. Both methods are related to Ackerman–Cox type corrections, where subtracting fluxes in a transparent spectral band from those in an absorbing band partially removes the radiative effects of horizontal inhomogeneity and allows the recovery of spatially resolved cloud absorption. The output of the two methods is different: while the subtraction method provides a contiguous record of recovered cloud absorption, the conditional sampling method yields a discrete set of data points where the vertical net flux divergence reliably estimates true cloud absorption.

KEYWORDS: Aircraft observations Short-wave radiation

1. INTRODUCTION

It is well understood that cloud absorption inferred from the difference between the measured net fluxes of two stacked aircraft below and above clouds is strongly affected by the uncertainties caused by cloud horizontal inhomogeneity. The simplest way to get rid of these uncertainties is to perform grand averages over flight legs (Valero *et al.* 1997); if flight legs are long enough (50–100 km), the averaging may lead to a trustworthy estimate of column absorption (Ramanathan and Vogelmann 1997). Even if spatial averaging yields a reliable estimate, the harvest of information on *true absorption* from such an expensive measurement program will be but a few numbers per day. This is insufficient for studying the dependence of true absorption on sun angle, cloud liquid water, cloud geometry, surface albedo, etc.

In this paper we discuss how to enhance the harvest of true absorption data from two-aircraft experiments using two related methods: (a) subtraction and (b) conditional sampling. Both methods offer an alternative to grand averaging. Both methods use additional spectral information assuming that, simultaneously with broad-band or narrow absorbing-band flux measurements, narrow non-absorbing-band measurements are also available (e.g. 0.5 μm measurements, see Valero *et al.* (1997)). Finally, both are related to the type of correction proposed by Ackerman and Cox (1981).

According to Ackerman and Cox, the difference between fluxes in a transparent (non-absorbing) spectral band (subindex 'tran') and in an absorbing band (subindex 'abs') is supposed to remove three-dimensional (3D) effects and lead to a correct

* Corresponding author: Joint Center for Earth Systems Technology, University of Maryland Baltimore County, 1000 Hilltop Circle, Baltimore, MD 21250 USA. e-mail: marshak@climate.gsfc.nasa.gov

absorption in the absorption band (see Rawlins (1989)):

$$A_{\text{sub}}(x) = \{R_{\text{tran}}(x) - R_{\text{abs}}(x)\} + \{T_{\text{tran}}(x) - T_{\text{abs}}(x)\}, \quad 0 \leqslant x \leqslant L. \tag{1}$$

Here, for simplicity, we assume no upward fluxes below clouds due to ground albedo and aerosol. A_{sub} is the Ackerman–Cox estimate of absorptivity, $R(x)$ and $T(x)$ are measurements of albedo and transmittance at point x, respectively; and L denotes the outer scale (for models) or flight-leg length (for measurements). Several aircraft experiments since 1981, notably Rawlins (1989) and Hayasaka *et al.* (1995), have used this correction; however, it was heavily criticized by Ramanathan and Vogelmann (1997).

2. Cloud model

A standard one-dimensional bounded cascade model (Cahalan 1994) is used to simulate horizontal distribution of cloud optical depth, $\tau_{\text{overcast}} > 0$. There are two variability parameters in this model: the first one, H_{bo}, determines its scaling behaviour while the second one, p, controls the variance-to-mean ratio. In addition to cloud inner structure, gaps are added in an ad hoc manner,

$$\tau_{\text{gappy}}(x) = b \max\{\tau_{\text{overcast}}(x) - a, 0\} \tag{2a}$$

where $a > 0$ and $b > 1$ are the constants uniquely derived from the assumed value of fractional cloudiness (Marshak *et al.* 1998a).

The variability of cloud top, $z_{\text{t}}(x)$, is simulated with a fractional Brownian motion (Mandelbrot 1977; for a simple algorithm used, see Peitgen and Saupe (1988)) *uncorrelated* with the internal bounded-cascade structure. Fractional Brownian motion is the generalization of a standard Brownian motion to parameters $0 < H_{\text{bm}} < 1$ that describe the 'roughness' of the function at small scales. The standard Brownian motion has parameter $H_{\text{bm}} = 1/2$.

Standard deviation of the cloud-top fluctuations has been chosen to match nine marine stratocumulus clouds observed by cloud radar during the Atlantic Stratocumulus Transition Experiment (Zuidema and Evans 1998). The range of the cloud-top variability is consistent with the Lidar In-Space Technology Experiment (Winker *et al.* 1996) measurements for stratus clouds (Loeb *et al.* 1998). Cloud base z_{b} is assumed flat, i.e. $z_{\text{b}}(x) \equiv z_{\text{b}}$.

Unlike Loeb *et al.* (1998), we assume the extinction coefficient $\sigma(x)$ to be independent of cloud-top variability and is calculated as

$$\sigma(x) = \tau_{\text{flat}}(x)/(\overline{z}_{\text{t}} - z_{\text{b}}), \quad 0 \leqslant x \leqslant L. \tag{2b}$$

Here by τ_{flat} we understand either τ_{overcast} or τ_{gappy}, and $\overline{z}$ means averaging over outer scale L. Thus the adjusted (bumpy-cloud) optical depth

$$\tau(x) = \sigma(x) \times \{z_{\text{t}}(x) - z_{\text{b}}\} = \tau_{\text{flat}}(x) \times \frac{z_{\text{t}}(x) - z_{\text{b}}}{\overline{z}_{\text{t}} - z_{\text{b}}}. \tag{2c}$$

Since the two random processes ($\tau_{\text{flat}}(x)$ and $z_{\text{t}}(x)$) are independent,

$$\langle \tau \rangle = \langle \tau_{\text{flat}} \rangle \tag{2d}$$

where $\langle \cdot \rangle$ means ensemble averaging. Note that Eq. (2d) is not necessarily true for any single realization.

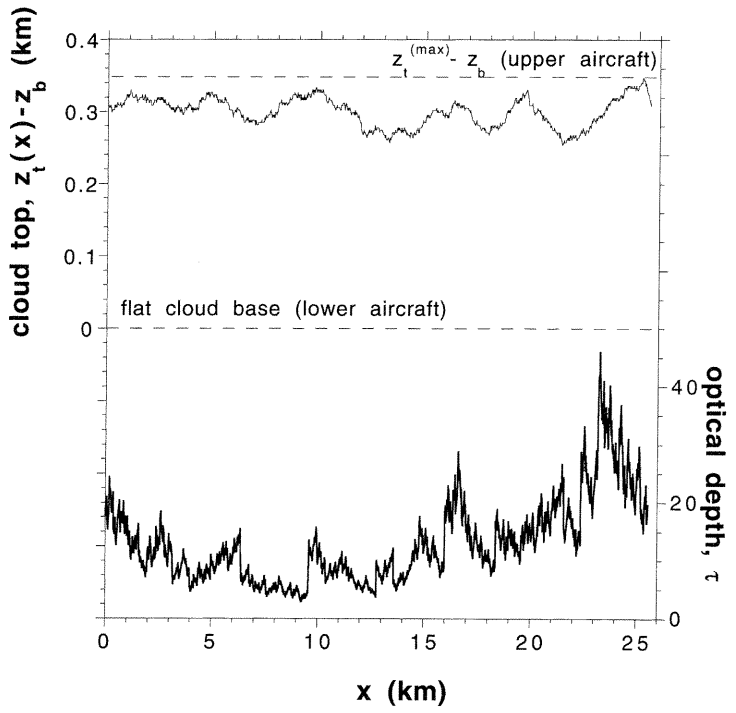

Figure 1. Cloud model. Upper curve is a realization of fractional Brownian motion for cloud-top altitude z_t, above cloud base, z_b, ($H_{bm} = 2/3$, mean = 0.3 km, standard deviation = 0.02), while lower curve is cloud optical depth τ as a product of a realization of the bounded cascade model ($H_{bo} = 1/3$, $p = 0.35$, mean = 13) and the normalized fractional Brownian motion as in Eq. (2c). See text for further explanation.

Figure 1 shows a realization of both $z_t(x) - z_b$ with $H_{bm} = 2/3$ and $\tau(x)$ as defined in Eq. (2c). Both lower (cloud base) and upper aircraft (maximal cloud top) flight legs are also indicated.

Note that the choice of fractional Brownian motion for the model of cloud-top fluctuations and its statistical independence from the horizontal variability of cloud optical depth do not have theoretical or observational justifications. (For example, Minnis *et al.* (1992) found that $z_t(x) - z_b$ is reasonably well correlated with the square root of $\tau(x)$.) However, the results below are not very sensitive to different statistical models simulating cloud-top variability; they are also robust against change of realizations and parameters.

Finally, in contrast to Marshak *et al.* (1997), where a narrow band around 0.94 μm with strong but horizontally *homogeneous* absorption (water vapour) and *inhomogeneous* scattering (liquid water) was chosen for detailed analysis, here we do not specify a spectral band but rather study the effect of different amounts of *inhomogeneous* absorption and *inhomogeneous* scattering (by liquid water) with no water vapour absorption. Six single-scattering albedos $\overline{\omega}_0$ were chosen for our simulations: 1.00, 0.999, 0.996, 0.99, 0.98, and 0.95 which cover the range currently calculated for pure liquid-water clouds in the short-wave spectrum. For simplicity, the same phase function and the same horizontal distribution of optical depth, $\tau(x)$, were used for all six cases; in addition, surface albedo was set to zero.

A new 'Local maximum cross-section' variance reduction Monte Carlo method is used for radiative-transfer calculations in these inhomogeneous cloud models. This

technique is especially efficient for broken clouds. Appendix A contains a description of the details of this method and compares it with our previously used 'Maximum cross-section' method (Marchuk *et al.* (1980), p. 9).

3. Absorption and Horizontal Fluxes

In the following we will distinguish between the 'true' and 'apparent' column absorption. The true absorption (fully accounting for 3D effects) is

$$A_{\text{true}}(x) = (1 - \overline{\omega}_0)\sigma(x) \int_{z_b}^{z_t^{(\max)}} \int_{4\pi} I(x, z; \mathbf{\Omega})\, \mathrm{d}\mathbf{\Omega}\, \mathrm{d}z,$$
$$0 \leqslant x \leqslant L, \quad \mathbf{\Omega} = (\Omega_x, \Omega_y, \Omega_z) \tag{3}$$

where radiance $I(x, z; \mathbf{\Omega})$ obeys the 3D radiative-transfer equation (see Eq. (A.1) in appendix A) and $z_t^{(\max)} = \max\{z_t(x), 0 \leqslant x \leqslant L\}$. The apparent absorption is defined as the difference between the vertical net fluxes at z_b and $z_t^{(\max)}$ (as measured in a two-aircraft experiment),

$$A_{\text{app}}(x) = \{1 - R(x)\} - \{T(x) - 0\}$$
$$= 1 - \int_{2\pi+} \Omega_x I(x, z_t^{(\max)}; \mathbf{\Omega})\, \mathrm{d}\mathbf{\Omega} - \int_{2\pi-} \Omega_x I(x, z_b; \mathbf{\Omega})\, \mathrm{d}\mathbf{\Omega} \tag{4}$$

and rigorously equals the true absorption only when the cloud is horizontally homogeneous. (Here $2\pi+$ and $2\pi-$ mean upper or lower hemisphere, respectively.) The difference between observed and real absorptions at each point x determines the vertically integrated horizontal flux:

$$H(x) = A_{\text{app}}(x) - A_{\text{true}}(x) \tag{5}$$

(Ackerman and Cox 1981; Rawlins 1989; Davis *et al.* 1997b; Marshak *et al.* 1998a; Titov 1998.) If outer scale L is large enough, the horizontal flux averaged over scale L vanishes; as a result,

$$\langle A_{\text{app}} \rangle \to \langle A_{\text{true}} \rangle, \quad \text{as } L \to \infty. \tag{6}$$

For all finite scales r, the spatially-averaged apparent absorption is at best an approximation to the spatially-averaged true absorption,

$$A_{\text{app}}(x, r) \equiv \frac{1}{r} \int_x^{x+r} A_{\text{app}}(x')\, \mathrm{d}x' \approx \frac{1}{r} \int_x^{x+r} A_{\text{true}}(x')\, \mathrm{d}x'$$
$$\equiv A_{\text{true}}(x, r), \quad 0 \ll r/L < 1. \tag{7}$$

As a spatially-averaged measure of the error at scale r, we define

$$E(r) = \frac{\int_0^L |A_{\text{app}}(x, r) - A_{\text{true}}(x, r)|\, \mathrm{d}x}{\int_0^L A_{\text{true}}(x)\, \mathrm{d}x} = \frac{\int_0^L |H(x, r)|\, \mathrm{d}x}{\int_0^L A_{\text{true}}(x)\, \mathrm{d}x}. \tag{8}$$

As an example, Fig. 2 shows $E(r)$ for three different solar angles θ_0 and $\overline{\omega}_0 = 0.99$. If $E^* > 0$ is an accuracy threshold, the solution of

$$E(r) = E^* \tag{9}$$

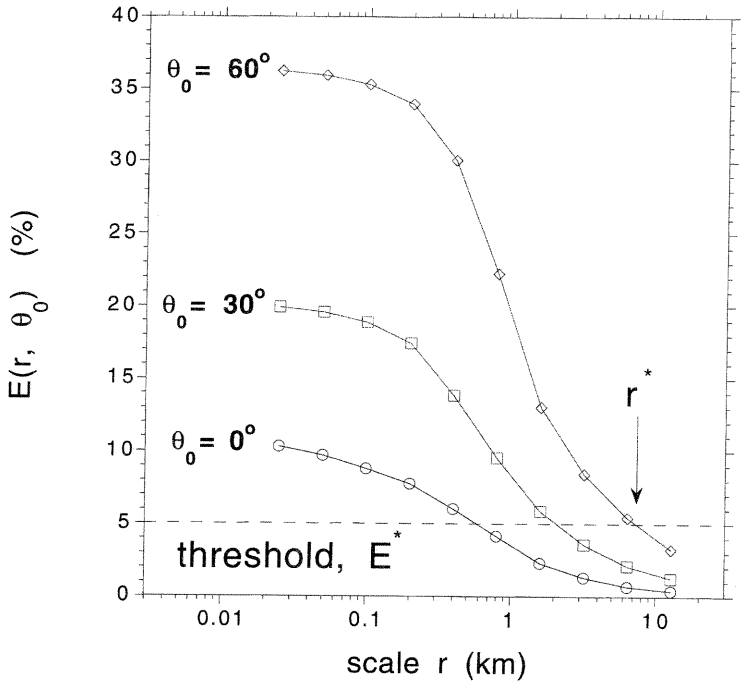

Figure 2. Relative error $E(r, \theta_0)$ (see Eq. (8)) for three different solar angles θ_0 and a single-scattering albedo $\overline{\omega}_0 = 0.99$. All curves are averaged over ten independent realizations of the cloud model. For illustrative purposes this case has the simplest possible horizontal inhomogeneity: variable cloud optical depth, no cloud-top variability and overcast sky.

gives us an averaging scale r^* that corresponds to the accuracy E^*. The integer part of the ratio L/r^* estimates the number of non-overlapping spatial intervals where the accuracy of spatially-averaged (over r^*) measurements of column absorption is better than E^*. It can happen that for an oblique illumination and a complex cloud structure/geometry, the ratio L/r^* for a typical 50 km flight leg is so small (even less than 1) that little information on column absorption is returned from the leg. Below we describe a procedure that modifies A_{app} by using bispectral information (Ackerman and Cox 1981; Rawlins 1989) and radiative smoothing theory (Marshak *et al.* 1995, 1998b; Davis *et al.* 1997b) with the goal of reducing r^* and thus retrieving more information from a flight leg.

4. SUBTRACTION METHOD

Let us now see how the statistics of spatial fluctuations in apparent absorption (4) compare with those of the true absorption (3). Figure 3 shows wave-number spectra $S(k)$ of a model of cloud optical depth and of true and apparent absorptions. Since the optical depth curve is a straight line on this log–log plot, the cloud model is scale-invariant. First, we see that true absorption fields A_{true} are also scale-invariant with an exponent (straight-line slope) similar to that of the optical depth field. This is true for all solar angles because the scaling properties of $\sigma(x)$ dominate on those of the integral of radiances $I(x, z; \mathbf{\Omega})$ (see Eq. (3)). By contrast, the apparent absorption field $A_{\text{app}}(x)$ has three distinct regimes: small scales where A_{app} is 'smoother' (smaller fluctuations) than A_{true}, intermediate scales where A_{app} is more variable and, finally, large scales where

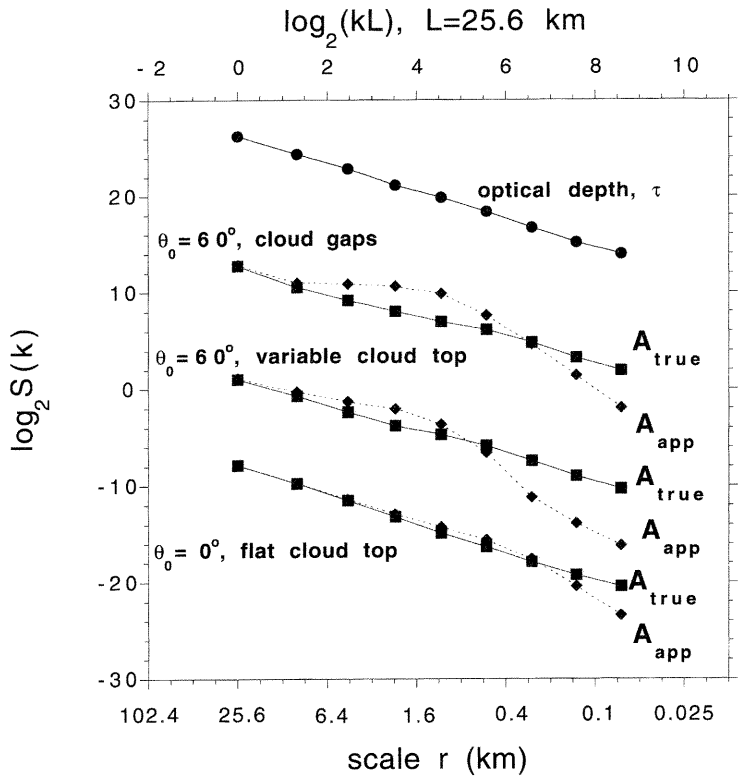

Figure 3. Octave averaged (Davis *et al.* 1996) wave-number spectra $S(k)$ of optical depth and of true and apparent absorption fields for a single-scattering albedo $\overline{\omega}_0 = 0.99$ and three cloud situations of increasing complexity. All statistics are averaged over ten realizations of the cloud model. For clarity, the two lower pairs are shifted down by 15 and 20, respectively.

both fields have similar fluctuations. These distinct scales are more pronounced for more oblique illumination and more complex cloud geometry.

It follows that to improve the verisimilitude of apparent absorption, we have to adjust the behaviour of A_{app} for small and intermediate scales. In this section we focus on the intermediate scales using net flux measurements in non-absorbing spectral bands.

Following Ackerman and Cox (1981) we assume that interactions between photons and inhomogeneous clouds are strongly correlated for absorbing and non-absorbing wavelengths. Then, if we subtract point-by-point the apparent absorption for a non-absorbing spectral band from the apparent absorption for absorbing spectral bands (as in Eq. (1)), we obtain a better approximation to A_{true}. The effect of this procedure is the most pronounced in cases of complex geometry and oblique illumination. Indeed the more geometrically complex cloud shapes are, the more horizontal fluxes are correlated in different spectral bands, since low-order scattering plays a dominant role in 'tracking' geometrical structures.

To illustrate the effect of the subtraction method for overcast clouds with variable cloud top, we plot in Fig. 4 a relative error $E(r)$ for low and high sun angles. As expected, the verisimilitude of A_{app} deteriorates with the increase of θ_0; as a result, $E(r, 60°)$ does not even converge to 0 as $r \to L$. This means that averaging over outer scale L may still not be sufficient for estimating the true column absorption. On the

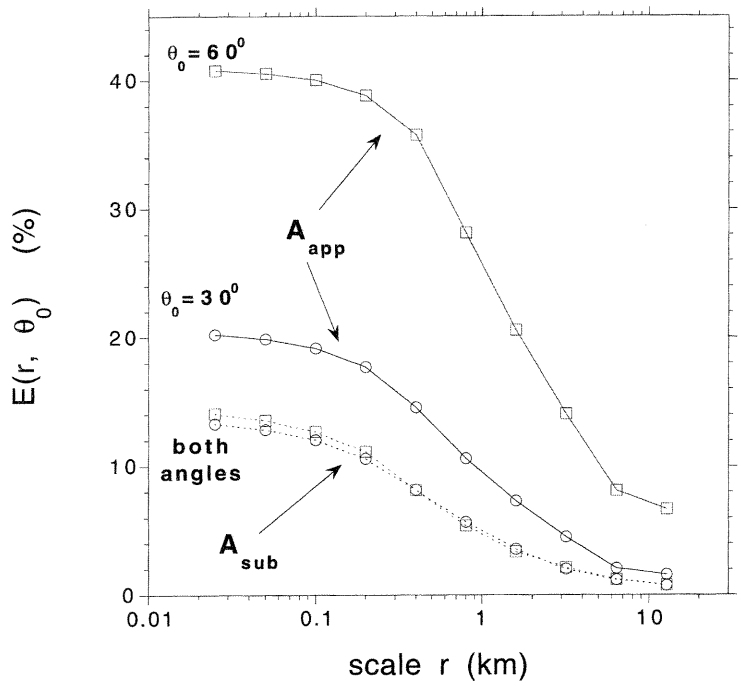

Figure 4. Relative error $E(r, \theta_0)$ (see Eq. (8)) for clouds with variable top under two solar angles: $\theta_0 = 30°$ (circles) and $\theta_0 = 60°$ (squares); single-scattering albedo $\overline{\omega}_0 = 0.99$. The lower curves represent the results of the subtraction method.

other hand, the subtraction method (two lower curves) makes $E(r) \to 0$ much faster and independently of θ_0. (Note that here and below all statistics are averaged over ten independent realizations of the cloud model.)

Figure 5 shows the entire wave-number spectrum for gappy clouds and $\theta_0 = 60°$. We see that the subtraction method removes strong fluctuations at intermediate scales and makes $A_{\text{sub}}(x)$ defined in Eq. (1) *a smoothed version* of $A_{\text{true}}(x)$. Our extensive calculations for many cases indicate that this statement is true for any solar angle and any complex cloud structure.

5. From a Smooth Field to a Rougher One

As we see from Fig. 5, A_{sub} is too smooth to be a good point-by-point approximation to A_{true}. To improve A_{sub} further we have to 'roughen' both small and intermediate scales. Radiative smoothing theory developed by Marshak *et al.* (1995) and applied by Davis *et al.* (1997a) to interpret the Landsat scale break in marine stratocumulus cloud, can be used as the main theoretical ground for the smoothing of a scale-invariant field like A_{true}. In this theory, one convolves a two-parameter family of gamma-type kernels, $G(x; \alpha, \eta)$, with $A_{\text{true}}(x)$ to approximate $A_{\text{sub}}(x)$, i.e.

$$A_{\text{sub}}(x) = A_{\text{true}}(x) * G(x; \alpha, \eta) \tag{10}$$

where G is an approximation to the radiative-transfer Green function, η is the characteristic radiative smoothing scale and α determines small-scale behaviour.

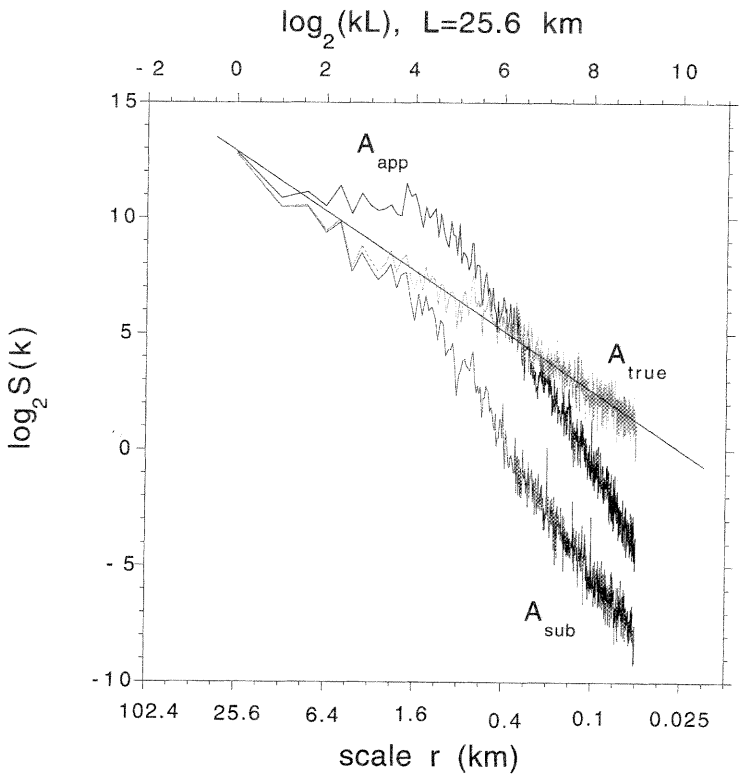

Figure 5. Wave-number spectra $S(k)$ of three cloud absorption fields for gappy clouds with a single-scattering albedo $\overline{\omega}_0 = 0.99$ and a solar angle $\theta_0 = 60°$. A least-squares fit illustrates scale-invariance of true absorption. See text for further explanation.

To retrieve A_{true} from A_{sub}, one has to deconvolve Eq. (10), equivalently, solve for A_{ret} the integral equation,

$$A_{\text{sub}}(x) = \int G(x - y; \alpha, \eta) A_{\text{ret}}(y)\, dy. \tag{11}$$

The solution A_{ret} of Eq. (11) will be an improved approximation to A_{true}. Note that Eq. (11) is an ill-posed problem that requires a regularization, as described by Marshak *et al.* (1998b).

Figure 6 illustrates the reduction of error produced by solving Eq. (11) for A_{ret} with $\eta = 0.175$ km and $\alpha = 1.2$. As an example, with a threshold $E^* = 3.5\%$ the new averaging scale $r^* = 0.4$ km is four to five times smaller than that for A_{sub}. This allows us to obtain at least four times more data points that reliably approximate true absorption. Finally, Fig. 7 complements Fig. 5 with the octave averaged wave-number spectrum of A_{ret}. We see that A_{ret} has the same wave-number spectrum as A_{true} down to $r^* = 0.4$–0.5 km; below that scale A_{ret} is much smoother than its true counterpart.

To provide a typical example of how this all works along a flight track, Fig. 8 shows a 3 km fragment of all four absorption fields: $A_{\text{true}}(x)$, $A_{\text{app}}(x)$, $A_{\text{sub}}(x)$, and $A_{\text{ret}}(x)$, with optical depth field $\tau(x)$ added below for reference. We see that the measured field, $A_{\text{app}}(x)$, the difference between net fluxes above and below the cloud, has intervals of 'negative absorption' which is anticorrelated with true absorption. This is because of the effect of cloud edges around 0.5 and 2 km which substantially increases transmittance

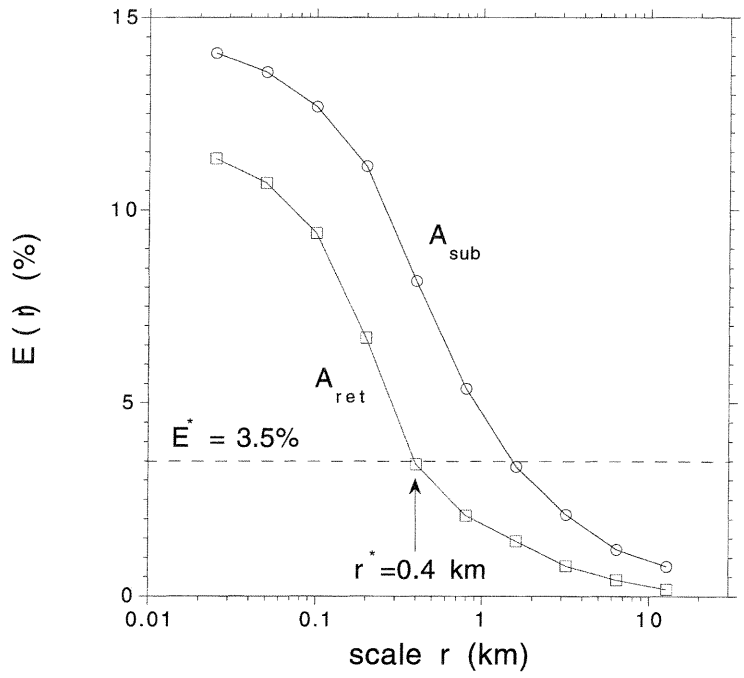

Figure 6. Relative error $E(r)$ after applying the subtraction procedure and then deconvolution (10). Clouds had variable top, $\overline{\omega}_0 = 0.99$ and $\theta_0 = 60°$; parameters of the Gamma distribution are $\eta = 0.175$ km and $\alpha = 1.2$, regularization parameter (see Marshak *et al.* 1998b) $\gamma = 0.0075$. Note that all three parameters are very stable and do not vary much with changing cloud geometry or illumination conditions. See text for explanation of symbols.

and thus decreases $A_{\text{app}}(x)$. After subtracting horizontal fluxes in transparent non-absorbing bands (Eq. (1)), the anticorrelation is removed, but the resulting field, $A_{\text{sub}}(x)$, is still too smooth and does not follow the fluctuations of $A_{\text{true}}(x)$ even for intermediate scales. The retrieved field, $A_{\text{ret}}(x)$, as the solution of Eq. (11), substantially improves the fit but only for intermediate scales, leaving small-scale fluctuations unmatched. Note the intervals of slightly negative absorption around 0.3 and 2 km.

The main reason for our inability to retrieve a proper fluctuation down to the smallest scales is the ill-posed nature of Eq. (11) (for explanations, see Marshak *et al.* (1998b)), although the intrinsically approximate nature of the convolution theory of radiative smoothing also plays a role. However, averaged over $r^* = 0.4$ km, $A_{\text{ret}}(x, r^*)$ is in good pixel-by-pixel agreement with $A_{\text{true}}(x, r^*)$. This is documented in Fig. 9 where both $A_{\text{app}}(x, r^*)$ and $A_{\text{ret}}(x, r^*)$ are plotted vs. $A_{\text{true}}(x, r^*)$ for 320 values of x.

6. CONDITIONAL SAMPLING

When one scatter plots $A_{\text{app}}(x)$ vs. $A_{\text{true}}(x)$ for each $x \in [0, L]$, there are many points that lie on the diagonal, even in the worst possible scenario (complex geometry, oblique illumination causing large horizontal fluxes). These points populate the whole diagonal and correspond to the entire range of cloud optical depths and different local geometrical shapes. If one could discriminate these points, the harvest of good data would be substantially increased; hence a natural question is: 'How can we capture just these points?'

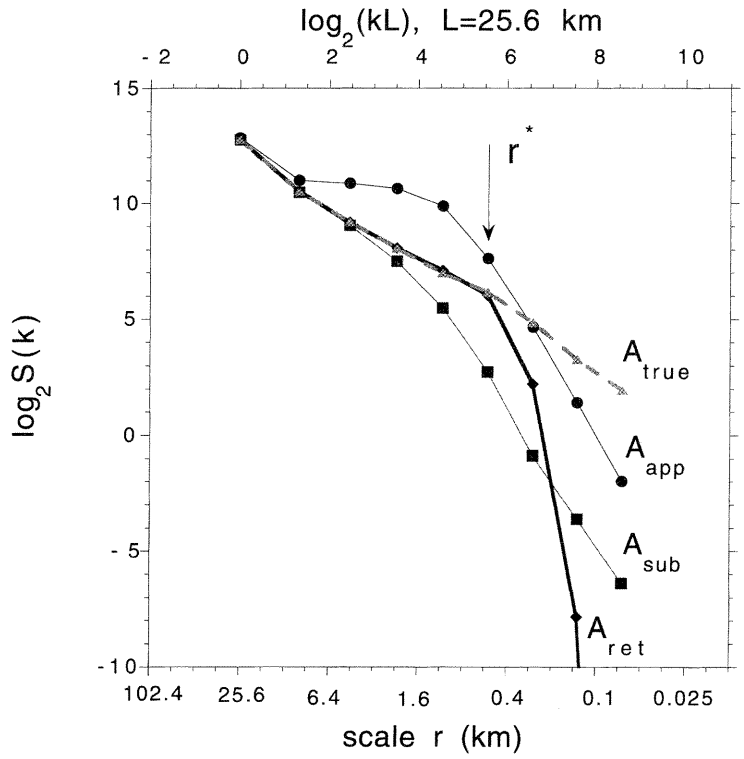

Figure 7. Octave averaged wave-number spectra $S(k)$ of four cloud absorption fields: A_{true}, A_{app}, A_{sub}, and A_{ret}. All parameters are the same as in Fig. 5. The arrow indicates scale $r^* = 0.4$–0.5 km; above this scale the wave-number spectra of A_{true} and A_{ret} coincide. See text for further explanation.

Based on Eq. (5), these points correspond to the locations with zero horizontal fluxes, i.e.

$$H_{\text{abs}}(x) = 0. \tag{12}$$

Now we assume that the points that have small horizontal fluxes in the absorbing spectral region are in the neighborhood U_ε of those points that have small (less than or equal to ε) horizontal fluxes in the transparent spectral bands, i.e.

$$U_\varepsilon = \{x: |H_{\text{tran}}(x)| \leqslant \varepsilon\}. \tag{13}$$

Taking into account that $H_{\text{tran}}(x)$ can be deduced from measurements as the vertical flux divergence in the transparent band,

$$H_{\text{tran}}(x) = \{1 - R_{\text{tran}}(x)\} - \{T_{\text{tran}}(x) - 0\}, \tag{14}$$

we propose a conditional sampling method, namely: use only those data-points that belong to U_ε. The apparent absorption at those points is presumably an accurate estimate of the true local absorption.

Figure 10 illustrates a scatter-plot of $A_{\text{app}}(x)$ vs. $A_{\text{true}}(x)$ for all $x \in [0, L]$ and for $x \in U_{0.01}$. The set $U_{0.01}$ consists of about 6% of all data points with cloud optical depths from 0 (clear sky) to over 100. These points occur all along the ten flight legs (realizations); each of them from 0 to 25.6 km. The single-scattering albedo $\overline{\omega}_0$ for this

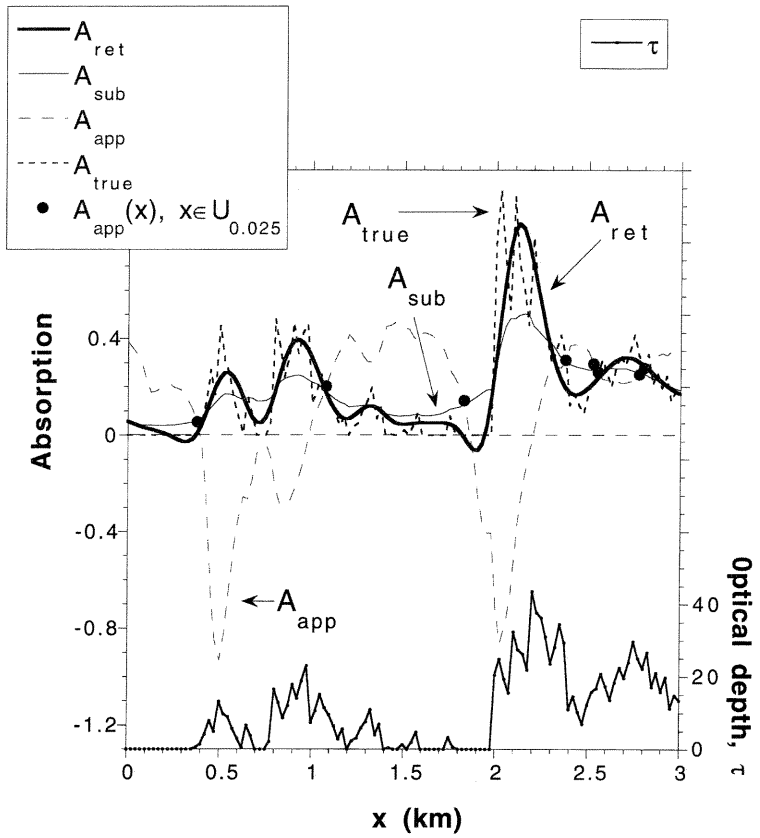

Figure 8. A 3 km fragment of four absorption fields: A_{true}, A_{app}, A_{sub}, and A_{ret}. Optical depth, τ, field is added for reference. All parameters are the same as in Fig. 5. Note that negative spikes in $A_{\text{app}}(x)$ around 0.5 and 2 km result from cloud edges and oblique illumination (solar beams come from the left side); hence large transmittance. Intervals of 'negative absorption' can be seen even in A_{ret}. In addition, eight bold circles on A_{app} correspond to those points where $|H_{\text{tran}}(x)| \leqslant 0.025$, i.e. $x \in U_{0.025}$. (For notations, see Eq. (13)). Note that the circles also intersect A_{true} as predicted by Eq. (15). See text for further explanation.

plot was chosen equal to 0.996 which corresponds to a narrow spectral band around 1.6 μm; this band is characterized by strong absorption by liquid water and very weak gaseous absorption.

In general, the assumption that $H_{\text{abs}}(x) = 0$ for $x \in U_\varepsilon$ is valid in a statistical sense only, even for relatively small ε. In the set $U_{0.01}$ plotted in Fig. 10, there are some outliers with $|H_{\text{abs}}(x)| > 0.1$ and, of course, A_{app} at these points is not a good estimate of A_{true}. However, the distribution of $H_{\text{abs}}(x)$ has a sharply-peaked, narrow, and close to symmetrical shape with mean 0.0013 and standard deviation 0.029 (Fig. 11). This tells us that about 60% of all points have $|H_{\text{abs}}(x)| \leqslant 0.02$, and at those points $A_{\text{app}}(x)$ is in good agreement with $A_{\text{true}}(x)$.

To illustrate the agreement, in Figs. 12(a) and 12(b) both $A_{\text{app}}(x)$ and $A_{\text{true}}(x)$ vs. $H_{\text{tran}}(x)$ are plotted for small optical depths (Fig. 12(a)) and intermediate ones (Fig. 12(b)). We see clearly that for a given cloud optical depth τ, a conditional sampling of $A_{\text{app}}(x)$ for x with $|H_{\text{tran}}(x)| \approx 0$ gives us an estimate of $A_{\text{true}}(x)$, i.e.

$$\{x : A_{\text{true}}(x) \cap A_{\text{app}}(x) \neq \emptyset\} = \{x: |H_{\text{tran}}(x)| \approx 0\}. \tag{15}$$

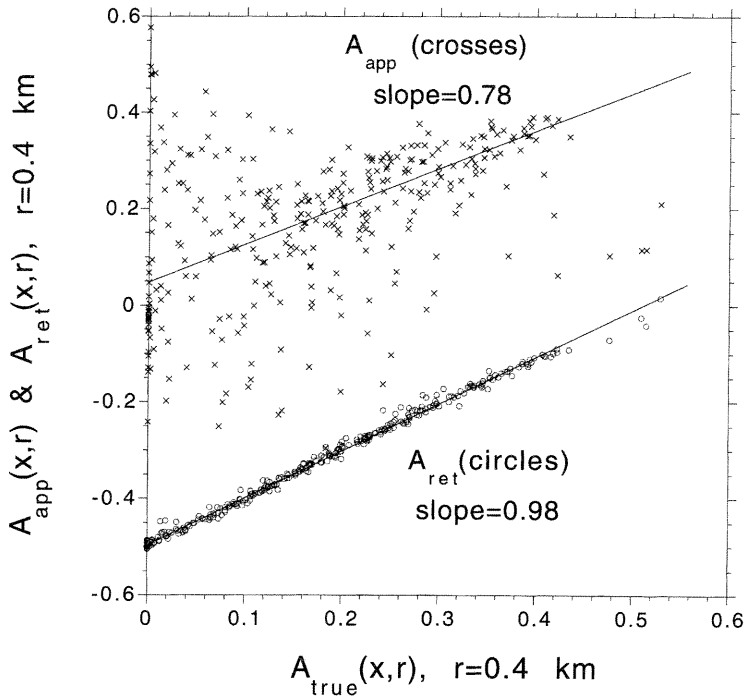

Figure 9. Scatter-plot of $A_{app}(x, r^*)$ and $A_{ret}(x, r^*)$ vs. $A_{true}(x, r^*)$ with $r^* = 0.4$ km. For clarity, values of A_{ret} are shifted down by 0.5. All parameters are the same as in Fig. 5. Straight lines are median fits (Press *et al.* 1993) which are closer to unity than least-squares fits. For comparison, least-squares fits for A_{app} vs. A_{true} and A_{ret} vs. A_{true} yield slopes 0.52 and 0.97, respectively. See text for further explanation.

Equation (15) is clearly illustrated in Fig. 8 with eight points $A_{app}(x_i)$ where $x_i \in U_{0.025}$ $(i = 1, \ldots, 8)$. We see that seven out of eight points also intersect A_{true}, i.e. they belong to $A_{true} \cap A_{app}$ as predicted by Eq. (15).

Alternatively, if we have measurements of $A_{app}(x)$ for only those points x that do not show $|H_{tran}(x)| \approx 0$, the extrapolation of them up (down) to the intersection with $|H_{tran}(x)| = 0$ gives us again a good estimate of A_{true} averaged over the neighbourhood of x with $|H_{tran}(x)| \approx 0$ (see Figs. 12(a) and 12(b)).

7. Summary and Discussion

Cloud absorption is extremely difficult to measure. If inferred from the difference between net fluxes at fixed altitudes below and above clouds measured by two stacked aircraft, the horizontally inhomogeneous cloud structure strongly affects the column absorption estimate. As a result, it is hard to distinguish between enhanced cloud absorption and natural variability in cloud structure, if spatial averaging is insufficient (Francis *et al.* 1997; Barker and Li 1997; Marshak *et al.* 1997).

However, it is important to realize that averaging over long flight legs is not a panacea. Perhaps the easiest way to illustrate this is to look at liquid water instead of absorption. Davis *et al.* (1996, Fig. 8(a)) shows how liquid water converges as one averages over longer and longer distances along flight segments in clouds specifically selected to look 'homogeneous'. While convergence is seen after perhaps 20–30 km,

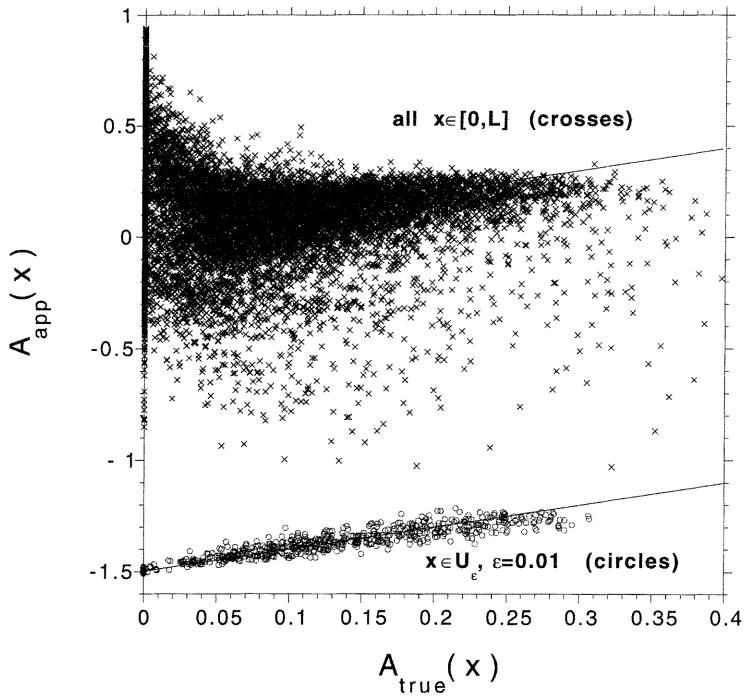

Figure 10. Scatter-plot of $A_{\text{app}}(x)$ vs. $A_{\text{true}}(x)$ for $x \in [0, L]$ and $x \in U_{0.01}$. For clarity, values of $x \in U_{0.01}$ are shifted down by 1.5. For notations, see Eq. (13). Ten independent realizations are used. The total number of $x \in [0, L]$ ($L = 25.6$ km) is $1024 \times 10 = 10\,240$ while the total number of $x \in U_{0.01}$ is 645. Gappy clouds with $\overline{\omega}_0 = 0.996$ and $\theta_0 = 60°$. Straight lines are the diagonals $A_{\text{app}}(x) = A_{\text{true}}(x)$. Median fitting for $A_{\text{app}}(x)$ vs. $A_{\text{true}}(x)$ for $x \in U_{0.01}$ (not shown) gives a slope of 0.924 while a least-squares fit gives a slope of 0.884. See text for explanation of symbols.

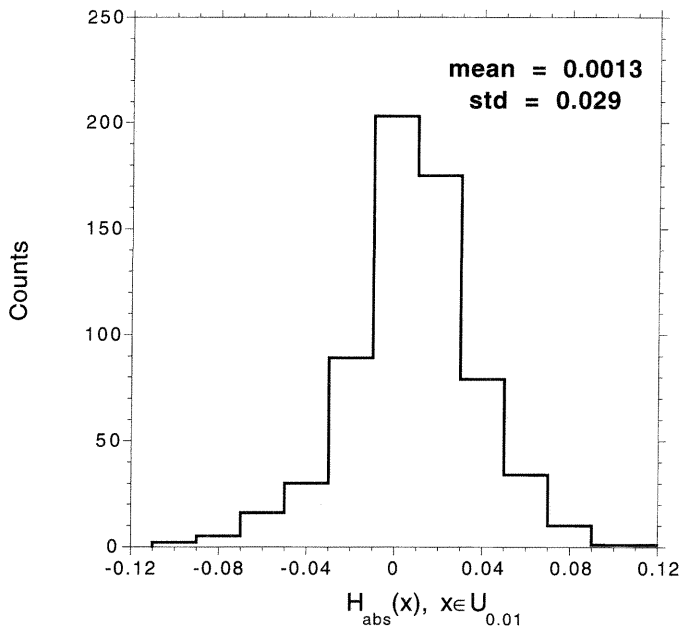

Figure 11. Histogram of $H_{\text{abs}}(x)$ for $x \in U_{0.01}$. For notation, see Eq. (13) and text for further explanation.

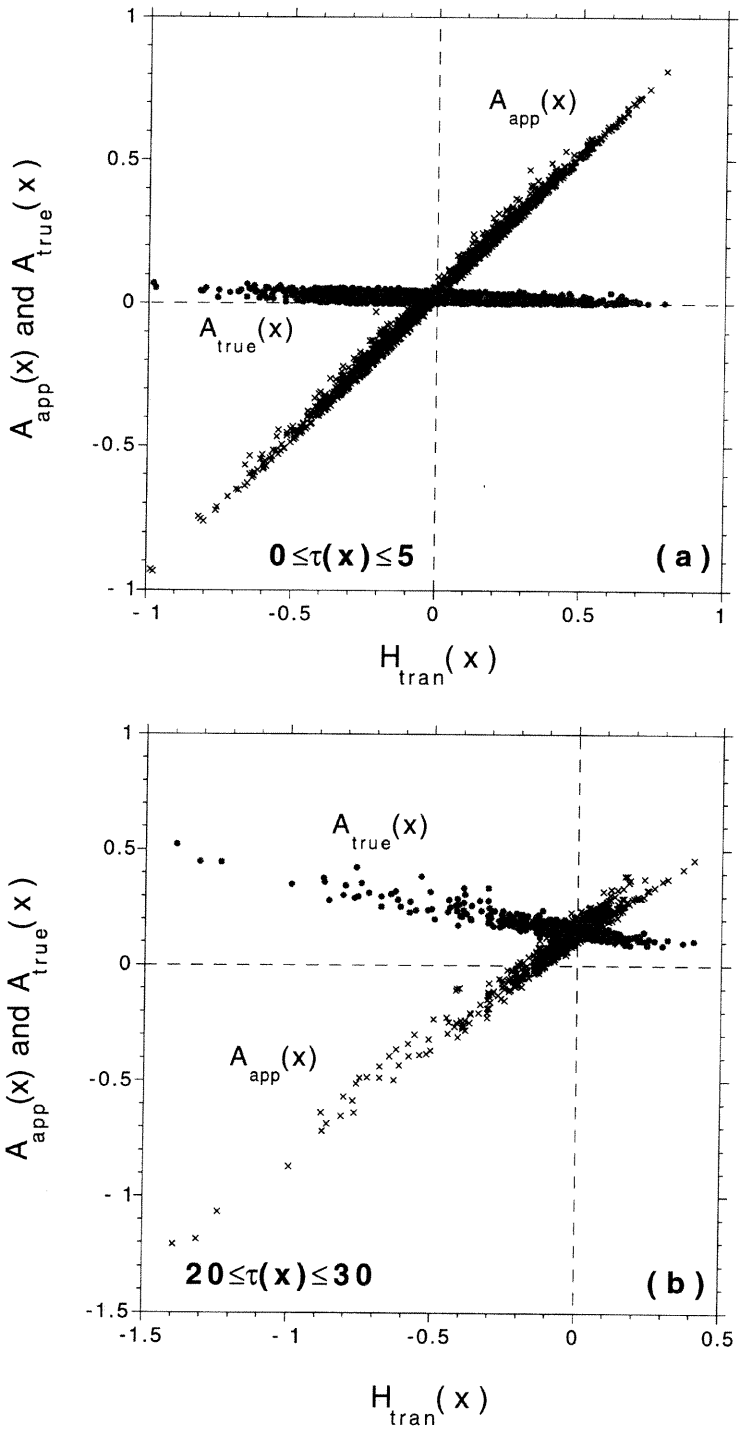

Figure 12. Scatter-plot of $A_{\text{app}}(x)$ (crosses) and $A_{\text{true}}(x)$ (bold circles) vs. $H_{\text{tran}}(x)$. All parameters are the same as in Fig. 10. (a) Optical depth $\tau \in (0, 5)$, and (b) optical depth $\tau \in (20, 30)$.

there is quite a bit of variation among the values to which they converged. The same thing will happen with absorption: first, if liquid water does not converge at all, then the absorption will not converge either, no matter how long the flight; second, if liquid water does converge, one may also see convergence in absorption, but the converged value is just a sample. A different cloud configuration, or even a different leg on the same day, will lead to a different sample value. Only a large number of such values can give any sense of the mean and the variability. Clearly, it would be much preferable to accumulate a large number of absorption samples on a given flight leg, in a short period of time, rather than arduously have to collect many samples over many days and try to deal with the knotty statistical heterogeneity questions which make such results more ambiguous.

Even if spatial averaging yields a reliable estimate of cloud absorption, the averaging requirements for two-aircraft measurements can be very strict (Evans 1997; Marshak *et al.* 1997) leading to a meagre data 'harvest' from such an expensive experiment. The present paper suggests two related ways of removing 3D effects and recovering true absorption and, as a result, increasing the data harvest.

Both methods use the idea originated by Ackerman and Cox (1981) that 3D effects in absorbing wavebands are similar to those in a transparent spectral band. The first method is to subtract (point by point) horizontal fluxes measured in a transparent band from the apparent absorption $A_{\rm app}$ measured in absorbing bands. This leads to $A_{\rm sub}$ which is less affected by the cloud horizontal inhomogeneity than the original $A_{\rm app}$. The field $A_{\rm sub}$ is, however, much smoother than $A_{\rm true}$, the true absorption field we want to retrieve. To 'roughen' $A_{\rm sub}$, we use a deconvolution with the radiative-transfer Green function, as approximated by a two-parameter gamma distribution. This is similar to the inverse non-local independent pixel approximation developed by Marshak *et al.* (1998b) for cloud property remote sensing.

We show that in cases of complex cloud structure and oblique illumination this roughened result allows the data harvest to be substantially increased. For example, averaging over 0.4 km of the roughened absorption field gives a 3–4% error; the same level of accuracy can only be achieved by averaging the originally measured difference between net fluxes over more than 10 km.

The second method (conditional sampling) uses only those data points that have no horizontal fluxes in a transparent band. The apparent absorption in these points in most cases will be a good estimate of a true absorption. This radically increases the data harvest beyond overall time and space averages.

Although not demonstrated, all techniques reported in this paper are robust against change of realizations and parameters in the cloud models. Indeed, the same general tendencies in $A_{\rm app}$ and $A_{\rm true}$ are observed in 2D vs. 1D horizontal variability, in presence vs. absence of vertical inhomogeneity, in variable vs. flat cloud top and, finally, Henyey–Greenstein vs. realistic phase function. However, our simulation assumes an 'ideal' two-aircraft experiment: lower and upper aircraft are stacked with no horizontal offset and no vertical separation between them and clouds.

Note that unlike Ackerman and Cox (1981), we do not require in-cloud absorption to be negligible in the 'visible' part of the solar spectrum. This assumption was found inconsistent with the recent Atmospheric Radiation Measurement (ARM) Enhanced Shortwave Experiment (ARESE) (Zender *et al.* 1997; Valero *et al.* 1997). The only assumption made in this paper is that, simultaneously with the total spectral broad-band measurements, narrow non-absorbing-band net flux measurements are available. As was shown by Valero *et al.* (1997), a narrow (10 nm width) channel centred at 0.5 μm satisfied this requirement during the ARESE.

In the near future, we will apply both methods to real-world data obtained during the ARESE for measuring short-wave absorption. However, the large vertical offset between upper aircraft and cloud top may not allow a straightforward application of our methods.

ACKNOWLEDGEMENTS

This work was supported by the Environmental Sciences Division of the US Department of Energy (under grant DE-A105-90ER61069 to the National Aeronautics and Space Administration's Goddard Space Flight Center) as part of the ARM program. We thank R. Pincus for fruitful discussions.

We dedicate this paper to the lasting memory of Professor Georgii Titov (1948–1998) who pioneered the topic of three-dimensional radiative transfer in clouds. His insightful remarks gave us the impetus for much of the research described in this paper.

APPENDIX

Advanced Monte Carlo technique

Our previous 3D Monte Carlo calculations for clouds achieved significant enhancement in speed by using the so-called 'Maximum cross-section method' (Marchuk *et al.* 1980) which involves transforming the radiative-transfer equation in a 3D scattering/absorbing optical medium $\mathbf{X}$ from

$$\mathbf{\Omega} \cdot \nabla I(\mathbf{x}; \mathbf{\Omega}) + \sigma(\mathbf{x}) I(\mathbf{x}; \mathbf{\Omega}) = \overline{\omega}_0 \sigma(\mathbf{x}) \int_{4\pi} P(\mathbf{\Omega} \cdot \mathbf{\Omega}') I(\mathbf{x}; \mathbf{\Omega}') \, \mathrm{d}\mathbf{\Omega}' \quad (\mathbf{x} \in \mathbf{X}), \quad \text{(A.1)}$$

where $\overline{\omega}_0$ is the single-scattering albedo and $P(\mathbf{\Omega} \cdot \mathbf{\Omega}')$ is the phase function, to

$$\mathbf{\Omega} \cdot \nabla I(\mathbf{x}; \mathbf{\Omega}) + \sigma_{\max} I(\mathbf{x}; \mathbf{\Omega}) = \sigma_{\max} \int_{4\pi} \left\{ \frac{\sigma(\mathbf{x})}{\sigma_{\max}} \overline{\omega}_0 P(\mathbf{\Omega} \cdot \mathbf{\Omega}') + \left(1 - \frac{\sigma(\mathbf{x})}{\sigma_{\max}}\right) \delta(\mathbf{\Omega} - \mathbf{\Omega}') \right\} I(\mathbf{x}; \mathbf{\Omega}') \, \mathrm{d}\mathbf{\Omega}' \quad \text{(A.2a)}$$

where $\sigma_{\max} = \max_{\mathbf{x} \in \mathbf{X}} \{\sigma(\mathbf{x})\}$ is the maximal volume extinction coefficient. Equation (A.2a) can be interpreted as the transport equation with constant extinction $\sigma_{\max}$ and a modified phase function:

$$\begin{cases} \overline{\omega}_0 P(\mathbf{\Omega} \cdot \mathbf{\Omega}'), & \text{with probability } \sigma(\mathbf{x})/\sigma_{\max} \\ \delta(\mathbf{\Omega} - \mathbf{\Omega}'), & \text{otherwise.} \end{cases} \quad \text{(A.2b)}$$

The advantage of this method is that the photon jumps immediately to its next scattering point instead of accumulating optical depth cell by cell. This makes the computer time almost insensitive to: (i) whether we use 1D, 2D, or 3D geometry; (ii) the variability of $\sigma(\mathbf{x})$ (except for very large $\sigma_{\max}$); and (iii) the number of cells (Marshak *et al.* 1995).

However, for very large $\sigma_{\max}$, the steps between scatterings become too small. Furthermore, for broken clouds, a photon takes the same small steps even across clear-sky regions; this substantially slows down calculations. To overcome these shortcomings, a 'Local maximum cross-section method', which explores the maximum extinction only along the photon beam from point $\mathbf{x}$ in the direction $\mathbf{\Omega}$, is developed. In other words,

Eq. (A.2a) is transformed to

$$\begin{aligned}\boldsymbol{\Omega}\cdot\nabla I(\mathbf{x};\,\boldsymbol{\Omega})+\sigma_{\max}(\mathbf{x};\,\boldsymbol{\Omega})I(\mathbf{x};\,\boldsymbol{\Omega})\\ =\sigma_{\max}(\mathbf{x};\,\boldsymbol{\Omega})\int_{4\pi}\left\{\frac{\sigma(\mathbf{x})}{\sigma_{\max}(\mathbf{x};\,\boldsymbol{\Omega})}\overline{\omega}_0 P(\boldsymbol{\Omega}\cdot\boldsymbol{\Omega}')\right.\\ \left.+\left(1-\frac{\sigma(\mathbf{x})}{\sigma_{\max}(\mathbf{x};\,\boldsymbol{\Omega})}\right)\delta(\boldsymbol{\Omega}-\boldsymbol{\Omega}')\right\}I(\mathbf{x};\,\boldsymbol{\Omega}')\,\mathrm{d}\boldsymbol{\Omega}'\end{aligned}\tag{A.3a}$$

where

$$\sigma_{\max}(\mathbf{x};\,\boldsymbol{\Omega})=\max\{\sigma(\mathbf{x}+t\boldsymbol{\Omega});\,t\geqslant 0,\,\mathbf{x},\,\mathbf{x}+t\boldsymbol{\Omega}\in\mathbf{X}\}.\tag{A.3b}$$

A modified phase function is similar to the one in Eq. (A.2b) where $\sigma_{\max}=\sigma_{\max}(\mathbf{x};\,\boldsymbol{\Omega})$.

A number of numerical comparisons between the Maximum cross-section and Local maximum cross section variance-reduction methods showed that for a cloud fraction of 60–90%, the latter method yields more than 40% speed up.

References

Ackerman, S. A. and Cox, S. K. 1981 Aircraft observations of the shortwave fractional absorptance of non-homogeneous clouds. *J. Appl. Meteorol.*, **20,** 1510–1515

Barker, H. and Li, Z.-Q. 1997 Interpreting shortwave albedo–transmittance plots: True or apparent anomalous absorption? *Geophys. Res. Lett.*, **24,** 2023–2026

Cahalan, R. F. 1994 Bounded cascade clouds: Albedo and effective thickness. *Nonlinear Processes in Geophys.*, **1,** 156–167

Davis, A., Marshak, A., Wiscombe, W. and Cahalan, R. 1996 Scale-invariance in liquid water distributions in marine stratocumulus. Part I: Spectral properties and stationarity issues. *J. Atmos. Sci.*, **53,** 1538–1558

Davis, A., Marshak, A., Cahalan, R. and Wiscombe, W. 1997a The LANDSAT scale-break in stratocumulus as a three-dimensional radiative transfer effect, implications for cloud remote sensing. *J. Atmos. Sci.*, **54,** 241–260

Davis, A., Marshak, A., Wiscombe, W. J. and Cahalan, R. F. 1997b Evidence for net horizontal radiative fluxes in marine stratocumulus. Pp. 809–812 in *IRS'96: Current problems in atmospheric radiation.* Eds. W. L. Smith and K. Stamnes. Deepak Publications, Hampton (Va), USA

Evans, K. F. 1997 The spherical harmonic discrete ordinate method: application to 3D radiative transfer in boundary layer clouds. Pp. 143–146 in *IRS'96: Current problems in atmospheric radiation.* Eds. W. L. Smith and K. Stamnes. Deepak Publications, Hampton (Va), USA

Francis, P. N., Taylor, J. P., Hignett, P. and Slingo, A. 1997 On the question of enhanced absorption of solar radiation by clouds. *Q. J. R. Meteorol. Soc.*, **123,** 419–434

Hayasaka, T., Kikushi, N. and Tanaka, M. 1995 Absorption of solar radiation by stratocumulus clouds: Aircraft measurements and theoretical calculations. *J. Appl. Meteorol.*, **34,** 1047–1055

Loeb, N. G., Várnai, T. and Winker, D. M. 1998 Influence of subpixel-scale cloud-top structure on reflectance from overcast stratiform cloud layers. *J. Atmos. Sci.*, **55,** 2960–2973

Mandelbrot, B. B. 1977 *Fractals: form, chance, and dimension.* W. H. Freeman, San Fransisco (Ca), USA

Marchuk, G., Mikhailov, G., Nazaraliev, M., Darbinjan, R., Kargin, B. and Elepov, B. 1980 *The Monte Carlo methods in atmospheric optics.* Springer-Verlag, New York, USA

Marshak, A., Davis, A., Wiscombe, W. and Cahalan, R. 1995 Radiative smoothing in fractal clouds. *J. Geophys. Res.*, **100,** 26247–26261

1997 Inhomogeneity effects on cloud shortwave absorption measurements: Two-aircraft simulations. *J. Geophys. Res.*, **102,** 16619–16637

Marshak, A., Davis, A., Wiscombe, W. J., Ridgway, W. and Cahalan, R. F. 1998a Biases in shortwave column absorption in the presence of fractal clouds. *J. Climate*, **11,** 431–446

Marshak, A., Davis, A., Cahalan, R. F. and Wiscombe, W. J. 1998b Nonlocal independent pixel approximation: Direct and inverse problems. *IEEE Trans. Geosci. Remote Sensing*, **36,** 192–205

Minnis, P., Heck, P. W., Young, D. F., Fairall, C. W. and Snider, J. B. 1992 Stratocumulus cloud properties derived from simultaneous satellite- and island-based measurements during FIRE. *J. Appl. Meteorol.*, **31,** 317–339

Peitgen, H.-O. and Saupe, D. (Eds.) 1988 *The science of fractal images*. Springer-Verlag, New York, USA

Press, W. H., Teukolsky, S. A., Vetterling, W. T. and Flannery, B. P. 1993 *Numerical recipies in FORTRAN*, 2nd ed. Cambridge University Press, New York, USA

Ramanathan, V. and Vogelmann, A. M. 1997 Greenhouse effect, atmospheric solar absorption and the earth's radiation budget: From the Arrhenius–Langley era to the 1990s. *Ambio*, **26,** 38–46

Rawlins, F. 1989 Aircraft measurements of the solar absorption by broken cloud fields: A case study. *Q. J. R. Meteorol. Soc.*, **115,** 365–382

Titov, G. A. 1998 Radiative horizontal transport and absorption in stratocumulus clouds. *J. Atmos. Sci.*, **55,** 2549–2560

Valero, F., Cess, R. D., Zhang, M. H., Pope, S. K., Bucholtz, A., Bush, B. and Vitko, J. 1997 Absorption of solar radiation by the cloudy atmosphere: Interpretations of collocated aircraft measurements. *J. Geophys. Res.*, **102,** 29917–29927

Winker, D. M., Couch, R. H. and McCormick, M. P. 1996 An overview of LITE: NASA's Lidar In-space Technology Experiment. *Proc. IEEE*, **84,** 164–180

Zender, C. S., Bush, B., Pope, S. K., Bucholtz, A., Collins, W. D., Kiehl, J. T., Valero, F. P. J. and Vitko, J. 1997 Atmospheric absorption during the Atmospheric Radiation Measurement (ARM) Enhanced Shortwave Experiment (ARESE). *J. Geophys. Res.*, **102,** 29901–29915

Zuidema, P. and Evans, K. F. 1998 On the validity of the independent pixel approximation for the boundary-layer clouds observed during ASTEX. *J. Geophys. Res.*, **103,** 6059–6074